Journal of Zhejiang University-SCIENCE A (Applied Physics & Engineering)
ISSN 1673-565X (Print); ISSN 1862-1775 (Online)
www.jzus.zju.edu.cn; www.springerlink.com
E-mail: jzus@zju.edu.cn

Influence of dry heating regime on the mechanical and shrinkage properties of reactive powder concrete*

Jin-tao LIU[1], Yang YANG[1], Chun-ping GU[†‡1], He-dong LI[2]

[1]*College of Architecture and Civil Engineering, Zhejiang University of Technology, Hangzhou 310014, China*

[2]*School of Civil Engineering and Architecture, Zhejiang Sci-Tech University, Hangzhou 310018, China*

[†]E-mail: guchunping@zjut.edu.cn

Received June 29, 2018; Revision accepted Sept. 14, 2018; Crosschecked Nov. 10, 2018

Abstract: The influence of the curing temperature (150 °C, 200 °C, 250 °C, and 300 °C) and curing time (4 h, 8 h, and 12 h) on the mechanical properties and shrinkage development of reactive powder concrete (RPC) was studied, and a curing regime for improving its mechanical properties is proposed. Test results show that the compressive and flexural strengths of specimens increase at curing temperatures of 200 °C to 250 °C, but decrease at curing temperature of 300 °C. Meanwhile, shrinkage measurement results indicate that the ultimate shrinkage of high-temperature cured RPC at 50% relative humidity (RH) is lower than in the control group. Scanning electron microscope results reveal that high-temperature curing improves the microscopic pore structure of RPC and makes the interfacial transition zone denser. Furthermore, the dry-heat curing regime can accelerate the cement hydration process, and tobermorite or xonotlite was found to be one of the major crystalline hydrates at high temperature.

Key words: High-temperature curing; Reactive powder concrete (RPC); Mechanical properties; Shrinkage
https://doi.org/10.1631/jzus.A1800394 **CLC number:** TU528

1 Introduction

Reactive powder concrete (RPC) is characterized by super high mechanical performance and excellent durability (Richard, 1994). Its compressive strength can reach 200 MPa, and the fracture energy of RPC reaches 40 000 J/m^2, which is 250-times that of ordinary concrete (Shi et al., 2015). RPC includes a large amount of binding material, such as granulated ground blast furnace slag, fly ash, and silica fume. The water to binder ratios of RPC are usually lower than 0.2. Therefore, only a small amount of the cementitious materials participate in the hydration reaction under the standard curing conditions (Cwirzen et al., 2008; Yazıcı et al., 2010; Park et al., 2015). However, most RPC components are prefabricated in the factory, and thus low manufacture costs and investment are very important for rapid construction. Recently, high-temperature curing technology has been used to activate the pozzolanic reaction of supplementary materials. Based on previous studies, steam-treated RPC at 60 °C results in a high compressive strength of 180 MPa (Park et al., 2015), and it achieves more than 200 MPa when the atmospheric steam curing temperature is increased from 70 °C to 90 °C (Cwirzen et al., 2008; Ishii et al., 2008). Similarly, autoclave curing has an obvious effect in increasing the flexural and compressive strengths of RPC specimens at an early age (Massidda et al., 2001; Prem et al., 2015). However, the steam and autoclave curing regime usually requires a long holding time (8–96 h) to

‡ Corresponding author

* Project supported by the National Natural Science Foundation of China (Nos. 51708501, 51478423, and 51778583), the China Postdoctoral Science Foundation (No. 2017M612028), and the Foundation of Zhejiang Provincial Key Laboratory of Space Structures (No. 201803), China

ORCID: Jin-tao LIU, https://orcid.org/0000-0002-1888-2529; Chun-ping GU, https://orcid.org/0000-0003-4102-0350

achieve target strength, and it also has a high requirement in terms of equipment. The existence of these problems is not conducive to accelerating the circulation of mould and increasing productivity.

To obtain high strengths of RPC in a relatively short time, a dry heating curing regime has been adopted to accelerate the binder hydration processes (Mostofinejad et al., 2016). The heat treatment processes modify the chemical composition of the cement hydrated products by reducing the CaO/SiO_2 and H_2O/CaO ratios, and they also lead to the development of longer C–S–H chains and accelerate the generation of tobermorite or xonotlite (Tam et al., 2010; Tam and Tam, 2013). Moreover, the relief of pressure through dry heating curing creates greater van der Waals forces with a closer configuration of capillary pores, making a denser cementitious matrix (Beglarigale et al., 2016). Shaheen and Shrive (2006) indicated that curing temperatures between 200 °C and 300 °C result in the highest compressive strengths. According to Peng et al. (2012), the compressive strength of RPC increases after exposure to 200 °C and 400 °C temperatures and decreases at 600 °C. In addition, some researchers have found that the compressive strength and fracture energy of RPC after heating from 200 °C to 300 °C increase more than at room temperature, but start to decrease as the temperature continuously increases (Felicetti et al., 2000; Tai et al., 2011; Zheng et al., 2012). According to these previous studies, the holding time and the maximum temperature are important factors responsible for the development of strength (Zdeb, 2017). However, the effects of the drying heat-treatment temperature and duration on the development of RPC strength are still unclear, and its mechanics need to be further discussed.

Shrinkage is another important factor affecting the mechanical and durability performance of RPC. The high volumes of cementitious materials in RRC make it susceptible to high drying and autogenous shrinkage at an early age (Habel et al., 2006; Tam et al., 2012; Yoo et al., 2013; Li and Xu, 2016; Yalçınkaya and Yazıcı, 2017), especially under high-temperature curing conditions. The early-age shrinkage of RPC after 48 h of heat curing (90 °C) was approximately 450 με (Li et al., 2017), and approximately 87% of the total autogenous shrinkage occurs during thermal treatment owing to the accelerated rate of early hydration at higher temperatures (Yanni and Youssef, 2009). Furthermore, the drying shrinkage increases as the curing temperature increases (Soliman and Nehdi, 2011). In contrast, Garas et al. (2009) reported that the shrinkage of RPC without thermal treatment is about six-times that of a specimen thermally treated at 90 °C for 48 h after 14 d of drying, and the specimens did not show any measurable free shrinkage after thermal treatment. Shen et al. (2018) observed a slight expansion after atmospheric steam curing. Most previous studies focused on the shrinkage of RPC under standard or atmospheric steam curing, and some prior studies have led to conflicting results. Thus, the effects of a dry-heat curing regime and external relative humidity (RH) on the shrinkage properties of RPC require further analysis.

Accordingly, RPC is designed and exposed to heat treatment with different maximum temperatures and curing times, and the effects of the curing condition and RH on the drying shrinkage of RPC are also investigated. The main objective of this study is to propose an appropriate dry heating regime for RPC. Additionally, the hydration products and microstructure of RPC after heat curing are analyzed.

2 Experimental

2.1 Materials and mix proportions

Ordinary Portland cement (P.O 52.5) which complies with ISO 679:1989 (ISO, 1989) was used in this experiment. Silica fume with the specific surface area of 20 m^2/g was added. Additionally, ground granulated blast furnace slag (GGBFS) with the specific surface area of 0.475 m^2/g and 28-d activity index of 105% was added as a dry powder. The chemical properties of Portland cement, silica fume, and slag are presented in Table 1. Quartz sand with a maximum particle size of 0.6 mm was added as filler. A commercial polycarboxylate-based superplasticizer (SP) with 30% solid content was used in this study. Steel fiber with a 12 mm length, 0.2 mm diameter, and a tensile strength of 2600 MPa was used as fiber reinforcement.

The mixture design of RPC used in this study is given in Table 2, and RPC mixes were produced using a Hobart mixer. The preparation of the RPC was as follows:

1. Cement, silica fume, slag, and quartz sand were mixed for about 2 min at a constant speed of 107 r/min.

2. SP and a half volume of water were added and mixed for about 5 min at a speed of about 107 r/min.

3. The remaining water was added and mixed for about 5 min at a constant speed of 198 r/min.

4. Steel fiber was added and mixed for about 2 min at a constant speed of 198 r/min.

The entire mixing process took about 15 min, and RPC was poured into the required molds when the mortar was ready. The fresh RPC paste was cast into steel molds and compacted using a vibrating table. Flexural (40 mm×40 mm×160 mm) and cubical (70.7 mm×70.7 mm×70.7 mm) specimens were prepared. Meanwhile, 40 mm×40 mm×160 mm prisms were cast for determining drying shrinkage. The specimens were removed from the mold after 24 h and cured in water at a temperature of 20 °C until reaching the appropriate age for dry-heat curing.

Table 1 Chemical properties of cementitious materials

Item	Chemical composition (%)		
	Cement	Silica fume	GGBFS
CaO	62.6	–	42.1
SiO_2	20.6	≥95	41.9
Al_2O_3	5.9	–	8.12
Fe_2O_3	3.9	–	2.13
MgO	1.76	–	4.07
Na_2O	0.18	0.13	0.11
K_2O	0.92	0.86	1.21
SO_3	2.18	–	0.26
Cl^-	0.015	–	0
Loss on ignition	1.94	≤3.63	0.1

Table 2 Mix design of RPC

Material proportion	Value
Cement (kg/m^3)	850
Silica fume (kg/m^3)	212
GGBFS (kg/m^3)	170
Quartz (kg/m^3)	1150
Superplasticizer (kg/m^3)	12
Water (kg/m^3)	187
Steel fiber (kg/m^3)	156
Fiber volume ratio (%)	2
Water/cement (W/C) ratio	0.22
Water/binder (W/C) ratio	0.15

2.2 Heating regime

The heat curing equipment used in this study was a high-temperature electric furnace with internal spatial dimensions of 600 mm×750 mm×500 mm (width×height×depth), the maximum temperature of which reached 400 °C. After demolding, the specimens were first placed in a water tank at 20 °C and cured for 48 h. The specimens were then put in the heat-curing equipment for 4 h, 8 h, and 12 h, during which time the curing temperature was maintained at 150 °C, 200 °C, 250 °C, and 300 °C. The curing conditions are shown in Fig. 1 and Table 3. It should be noted that a sudden change in temperature might cause the specimens to undergo thermal stress during the curing process, and thus the speed of the temperature increase was set to 1 °C/min. Finally, the heating equipment was turned off and the specimens were continuously cooled to room temperature.

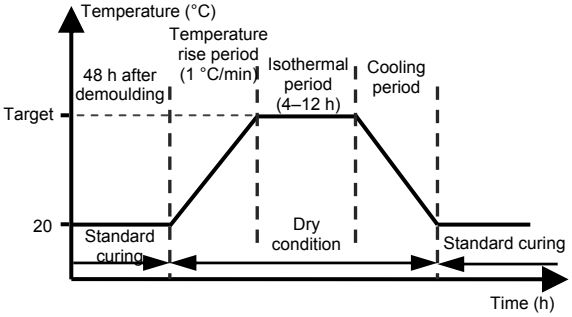

Fig. 1 Dry heat curing regimes used in this study

Table 3 Variables of curing conditions

Sample No.	Delay time (h)	Curing temperature (°C)	Curing time (h)	Moisture condition
R	–	20	–	Water
D15T8	48	150	8	Dry
D20T4	48	200	4	Dry
D20T8	48	200	8	Dry
D20T12	48	200	12	Dry
D25T4	48	250	4	Dry
D25T8	48	250	8	Dry
D25T12	48	250	12	Dry
D30T8	48	300	8	Dry

High temperature and a dry atmosphere may bring the volume change of reactive powder concrete

specimens. Therefore, the influence of high-temperature curing on the morphologies of specimens was studied by microscope (300×) after thermal treatment. However, there were no obvious cracks observed during the study. In addition, the surface color of the RPC specimens showed no significant changes after different high-temperature curing, as shown in Fig. 2. With the increase in curing time and temperature, the surface color of the RPC specimen changed slightly from grey to grey-brown.

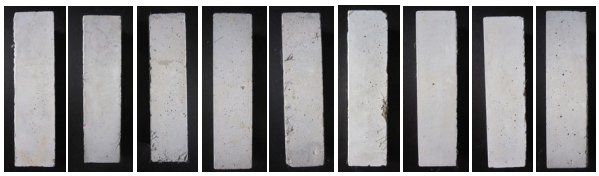

Fig. 2 Surface color of RPC samples with different curing regime

2.3 Test method

The compressive strength was tested at a loading rate of 0.4 mm/min using a 1000 kN Instron test platform at day 7 and day 28. A three-point bending test was carried out to quantify the effects of the curing regime on the flexural strength, and specimens aged 7 d and 28 d were tested using a 250 kN Instron universal material test machine at a loading speed of 0.2 mm/min, where the distance between the two supports was 120 mm. To study the effects of RH on the drying shrinkage properties of RPC, the shrinkage specimens were stored in a controlled environment of (90±10)% RH and (50±10)% RH separately before and after high-temperature curing. It should be noted that tests were conducted on three specimens each time, and measurements of the changes in specimen length were recorded daily, weekly, and monthly for a six-month period.

3 Experimental results

3.1 Test method

The effects of dry-heat curing time and temperature on strength development were investigated and are described in this section. Table 4 shows the average flexural and compressive strengths of the specimens at day 7 and day 28. Differing from conventional concrete, the high amount of cementitious material and low water/binder ratio increase the strength of the RPC matrix. The compressive strength of the RPC increased to 110 MPa under 7 d of standard curing and reached 163 MPa at day 28. High-temperature curing can dramatically improve the compressive strength of RPC. Using the same dry-heating time (8 h), the early-age compressive strengths of RPC were improved when the curing temperature increased, which resulted in increases of 32.6%, 49.1%, and 54.3% of the specified strength for curing temperatures of 150 °C, 200 °C, and 250 °C, respectively. However, the increase was a mere 30.2% when the curing temperature reached 300 °C. Similarly, the compressive strengths of D15T8, D20T8, D25T8, and D30T8 were increased 5.5%, 10.7%, 9.3%, and 1.1%, respectively, when compared with the control group at day 28. On the other hand, the compressive strength of the RPC was also affected by the dry-heat curing time. When the curing temperatures were 200 °C and 250 °C, the strength of the specimens first increased and then decreased with the increase in curing time. Generally, the 28-d compressive strength of RPC under standard curing can be achieved and even exceeded in about 7 d through dry-heat curing.

As shown in Table 4, the 7-d flexural strength of the RPC was significantly affected by the curing temperature, whereas both the cracking and ultimate strengths were improved at a high curing temperature. The results indicate an increase in the 7-d cracking strength from 1.1 to 8.8 MPa after the different curing regimes. In the case of D25T12 mortar, the 7-d ultimate flexural strength reached 35.3 MPa; furthermore, the 28-d cracking and ultimate flexural strengths were improved by 57.7% and 22.8%, respectively. Flexural load-deflection curves of RPC after different curing conditions are shown in Fig. 3, and these curves are similar among the different groups. First, the steel fibers and matrix sustained the internal load as a whole before it reached the initial-cracking, and the internal micro-cracks in the RPC matrix then gradually developed into macroscopic cracks and several cracks appeared in the area when subject to tensile stress. Finally, an increasing number

Table 4 Mechanical properties of RPC under different curing conditions

Sample	Compressive strength (MPa)		Flexural strength (MPa)				Toughness index		E_f (GPa)
	7-d	28-d	7-d cracking strength	7-d ultimate strength	28-d cracking strength	28-d ultimate strength	I_5	I_{10}	
R	110.3±12.5	163.0±6.6	18.2±2.8	26.8±2.8	20.8±3.3	30.7±2.5	4.55	8.28	5.66
D15T8	146.3±10.7	171.9±5.9	25.0±5.0	30.3±5.7	27.2±1.6	34.3±3.2	5.90	11.09	6.23
D20T4	160.4±14.0	173.0±0.8	24.0±2.0	30.8±1.3	28.3±1.5	35.0±1.0	6.70	12.96	6.81
D20T8	164.5±16.3	180.5±2.9	21.0±1.7	27.3±4.5	21.3±1.9	33.7±2.1	6.13	11.88	6.44
D20T12	168.1±12.2	174.6±3.6	24.7±1.5	30.3±3.8	32.8±0.8	37.7±3.8	5.42	10.59	6.37
D25T4	167.6±0.7	178.1±4.5	19.3±4.2	26.3±1.8	26.2±2.8	31.0±5.0	5.79	11.30	6.92
D25T8	170.2±24.5	181.6±8.6	23.7±3.5	33.0±2.6	26.0±4.2	32.0±2.6	6.64	13.43	7.16
D25T12	171.0±11.6	174.0±1.8	27.0±4.4	35.3±2.1	29.3±2.1	34.7±6.1	5.36	9.14	6.27
D30T8	143.6±12.5	164.8±6.5	20.7±2.3	28.3±4.1	23.3±0.4	32.8±1.1	4.79	8.51	5.47

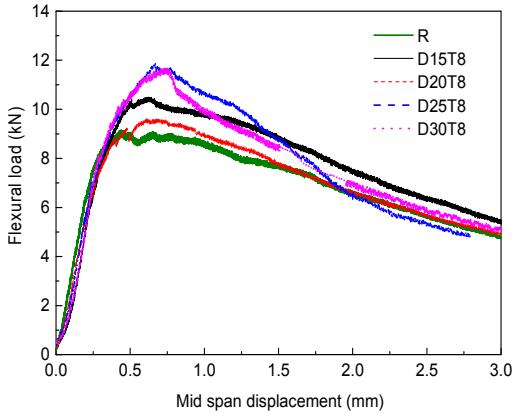

Fig. 3 Flexural load–mid span displacement relationship of RPC mixtures at day 7

of steel fibers were pulled out and the flexural stress decreased gradually with the growth of the cracks, and the specimen eventually broke. The dry-heat curing regimes positively affected the flexural strength of the RPC owing to the improvement in bond strength between the matrix and steel fibers. There were sudden load decrements and increments in the descending branch of the curves, which were caused by the sudden removal of the steel fibers.

The flexural modulus E_f and the toughness indexes (I_5 and I_{10}) were evaluated at day 28, and the results are summarized in Table 4. According to ASTM C1018 (ASTM, 2006), the toughness indexes I_5 and I_{10} are the values obtained by dividing the area up to a deflection of 3 and 5.5 times the first crack deflection by the area up to the first crack. Toughness indexes reflect the ability of energy consumption of RPC after cracking. Compared with the control group, the flexural toughness of RPC with temperature curing was remarkably improved. The toughness indexes I_5 and I_{10} of D25T8 were increased by 45.9% and 62.2%, respectively. However, the increase was small when the curing temperature reached 300 °C. As shown in Table 4, the flexural modulus of the RPC was also significantly affected by the curing temperature. The flexural modulus E_f of D15T8, D20T8, and D25T8 was increased by 10.1%, 13.8%, and 26.5%, respectively, when compared with control group. However, the elasticity modulus of RPC was decreased by 3.4% when the specimens were exposed to temperatures up to 300 °C.

3.2 Drying shrinkage

The drying shrinkage of RPC can result in a cracking of the concrete, thereby decreasing its integrity, anti-seepage, durability, and structural safety. The very high cement content and low water/binder ratio of RPC cause a rapid hydration reaction and shrinkage; therefore, specifying the drying shrinkage of RPC for long-term performance is very necessary. In general, the drying shrinkage of RPC is caused by the withdrawal of water into the surroundings from the hardened concrete stored in unsaturated air, and is affected by the age of the concrete, the mixture constituents, the curing temperature, the relative humidity, and certain other factors. Considering that RPC has been applied to different engineering projects, two different environmental humidity levels, 90% RH and 50% RH, were applied to explore the effects

of RH on the shrinkage of RPC. The shrinkage strain $\varepsilon(t)$ at an age of concrete is calculated using Eq. (1), which is a modification of the equation recommended in ACI 209R (ACI, 1997).

$$\varepsilon(t) = \varepsilon_{\text{fin}} t / (A + t), \tag{1}$$

where ε_{fin} is the ultimate shrinkage strain, A is a variable defining the shape of the curve, and t is the time after shrinkage is considered, that is, after the samples are demolded. The value of A and the correlation coefficient R^2 of each group are shown in Table 5.

Table 5 shows the ultimate shrinkage for all RPC mixtures. It can be observed that the ultimate shrinkage strains of the reference RPC under 90% RH and 50% RH are 324.0 με and 1083.3 με, respectively, and the results from Eq. (1) can fit the shrinkage development process quite well. With the exception of the D30T8 group, the drying shrinkage values of all specimens were less than 600 με under 90% RH. It can be seen from Table 5 that, with 8 h of dry heating, the ultimate drying strains of the specimen increased as the curing temperature increased, which resulted in 437.5 με, 531.3 με, 562.5 με, and 708.3 με for curing temperatures of 150 °C, 200 °C, 250 °C, and 300 °C, respectively. However, the mixtures in 50% RH showed much higher drying strains compared to those of the mixtures in 90% RH, and the effects of the curing temperature on the drying strains at 50% RH exhibited the same trend.

The drying strain development of RPC at 50% RH and 90% RH is shown in Fig. 4 as the average values from three specimens for each group. It can be clearly seen that most of the drying shrinkage occurred during the first few days after demolding. High-temperature cured RPC showed a faster shrinkage during the first few days, but then slowed down. Taking the D20T8 specimens as an example, after day 4, the shrinking values at 90% RH and 50% RH were 439 με and 500 με, whereas in the control group they were 156 με and 393 με, respectively. The drying shrinking values of the control group were significantly lower than those of the other groups at an early age; however, the shrinkage of a specimen after high-temperature curing grew slowly or even fell with an increase in age, particularly under 50% RH conditions.

It is worth noting that, except for the D30T8 and D25T12 groups, the ultimate shrinkage of high-temperature cured RPC at 50% RH was lower than in the control group. For example, the ultimate shrinkage of D20T4 and D25T4 decreased by 26.9% and 42.3%, respectively. Although D20T8 and D25T8 showed higher early shrinkage with an increase in curing time, the ultimate shrinkage of these two groups was lower than that of the control group. High-temperature curing can accelerate the evaporation of water from the samples and decrease the chemically bound water significantly, and thus an increase in shrinkage can be triggered as a result of a higher curing temperature.

3.3 Microstructures of RPC

The macroscopic properties of RPC are related to its microstructures, and are the key to optimizing RPC, particularly with respect to the durability and strength. Herein, the composition of the C–S–H

Table 5 Drying shrinkage of RPC

Sample	90% RH			50% RH		
	Ultimate shrinkage (με)	A	R^2	Ultimate shrinkage (με)	A	R^2
R	324.0	7.2957	0.969	1083.3	4.2216	0.987
D20T4	416.7	2.3987	0.858	791.7	1.6367	0.746
D25T4	458.3	2.6385	0.860	625.0	1.5963	0.786
D15T8	437.5	0.6392	0.900	718.8	3.2131	0.943
D20T8	531.3	1.7776	0.932	770.8	2.3597	0.948
D25T8	562.5	1.0039	0.927	895.8	1.1525	0.937
D30T8	708.3	0.0739	0.555	1354.2	0.7949	0.797
D20T12	468.8	1.3864	0.786	833.3	1.3606	0.824
D25T12	592.3	1.4703	0.710	1125.0	1.5186	0.852

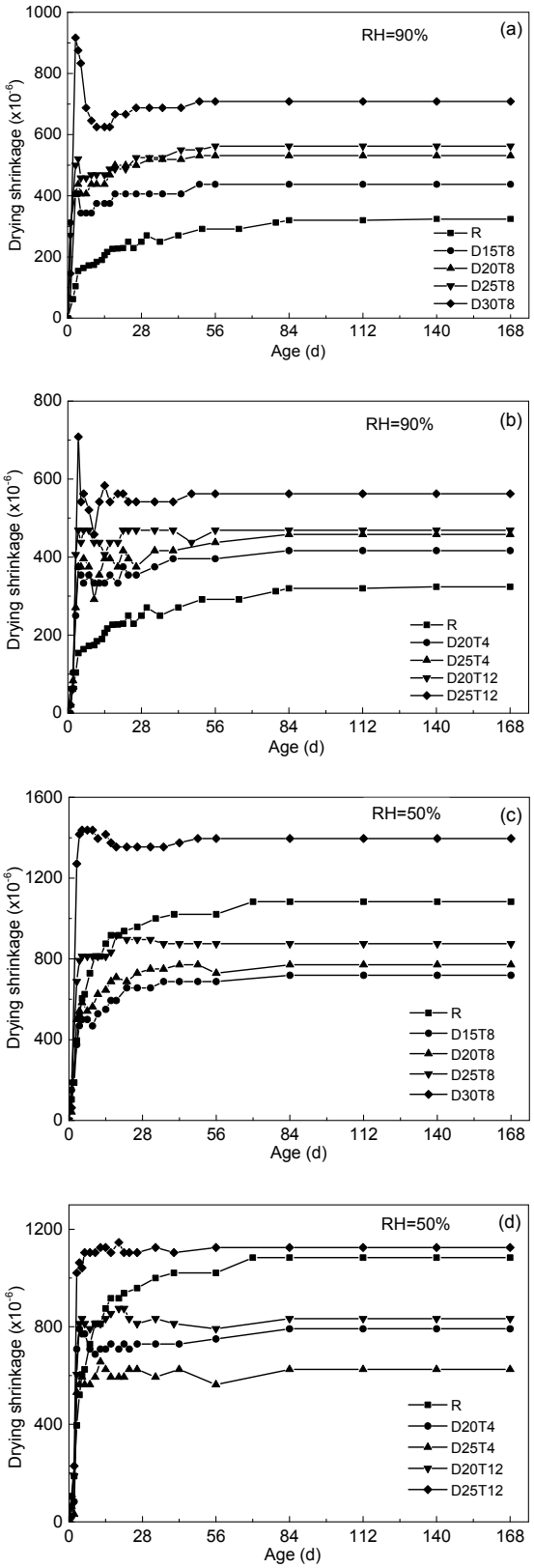

Fig. 4 Drying shrinkage of RPC at 90% RH (a, b) and 50% RH (c, d)

product phases was studied using scanning electron microscope (SEM). The matrix phase of the reference RPC predominantly consists of unhydrated cement grains, and stratiform $Ca(OH)_2$ is present in the microstructure owing to the relatively high cement content. Some spherical pores also exist in RPC and are generally empty or filled with tobermorite- or jennite-like structures, as shown in Fig. 5a. However, with heat treatment, the formation of C–S–H phases fills in the small pores and leads to a denser microstructure. Fig. 5c shows a micrograph of RPC cured at high temperature and reveals a compact formation of hydration products and a reduced amount of $Ca(OH)_2$ crystals.

Moreover, it shows that the bonding of the interfacial transition zone between the aggregate and cement paste becomes stronger. By comparing Figs. 5b and 5d, it appears that the reaction products were stuck to the surface of the steel fibers at high temperature, whereas the surfaces of the steel fibers in the R group were quite smooth. Researchers also reported that the drying of C–S–H creates greater van der Waals forces with a closer configuration of capillary pores, which may compact the fiber–matrix interface (Aydın et al., 2008; Beglarigale et al., 2016).

An SEM micrograph of RPC samples exposed to a temperature of 200 °C did not show any distinct changes in morphology, whereas the morphology of the RPC matrix showed deformed $Ca(OH)_2$ crystals and some voids at 300 °C. In addition, a 300 °C curing temperature was shown to lead to the predominance of drying-shrinkage microcracks (arrow mark), as indicated in Fig. 5f. These microcracks may be due to the non-uniform drying shrinkage of the matrix, which is caused by the moisture gradient across the specimen during high-temperature treatment (Hwang and Young, 1984). The RPC matrix was unable to obtain externally available curing, and thus capillary pore water was consumed. This self-desiccating action leads to microstructure stresses during drying, which may increase the cracking of RPC.

3.4 X-ray diffraction analysis

X-ray diffraction analyses were conducted to identify the crystalline solid phases of RPC, the diffraction patterns of which are shown in Fig. 6 for the

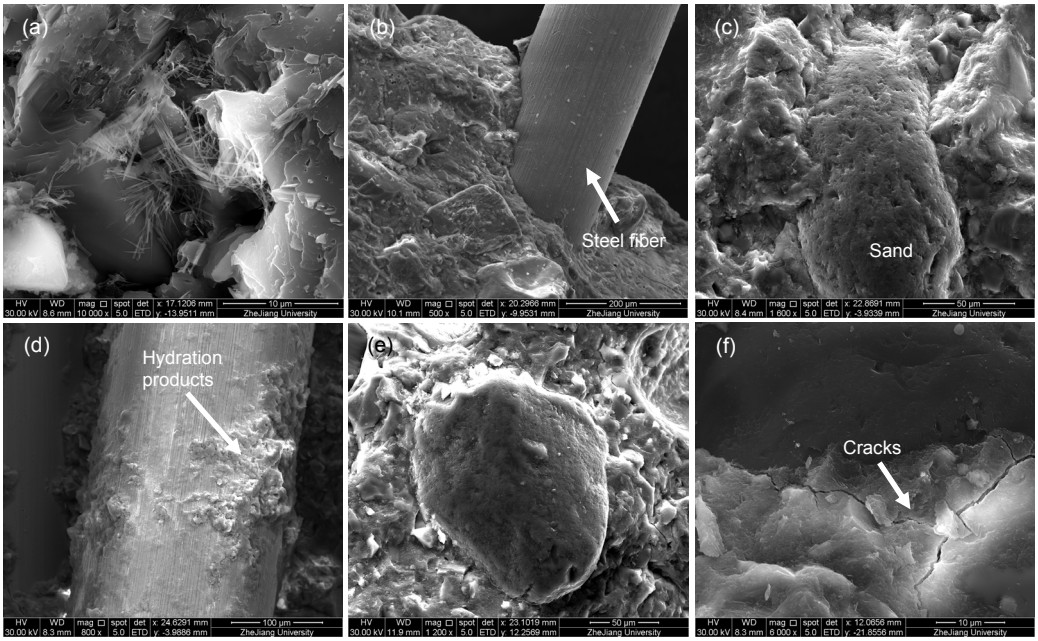

Fig. 5 SEM micrographs of control specimen (a, b), D20T8 (c, d), and D30T8 (e, f) groups

samples after 7 d. The main crystalline phases found in the RPC were unhydrated cement particles, belite (C_2S), ettringite, and calcium hydroxide ($Ca(OH)_2$). The high content of silica fume and slag consumed most of the CH crystals produced during hydration in the high-temperature curing regime, and these crystals were converted to strong C–S–H gel (Reda et al., 1999). However, most of the C–S–H phases remain amorphous, and were difficult to detect in X-ray diffraction (XRD) analyses (Wang et al., 2015). Compared to the XRD pattern of the reference group, the diffraction peaks of $Ca(OH)_2$ gradually reduced. This is mainly due to the reaction between supplementary cementitious materials and $Ca(OH)_2$ during the high-temperature curing stage, and the $Ca(OH)_2$ content decreased with the increase in curing temperature. This suggests that the heat treatment accelerates the early stage hydration of the silica fume and slag.

Ettringite formed during the early hydration and was present in the pore solution or adsorbed in the C–S–H structure; in addition, it was found that the heat treatment clearly reduced the formation of ettringite, as shown in Fig. 6a. Previous studies have indicated that the transformation of amorphous hydrates into crystalline products improved the microstructure of RPC (Lehmann et al., 2009; Chen et al., 2018).

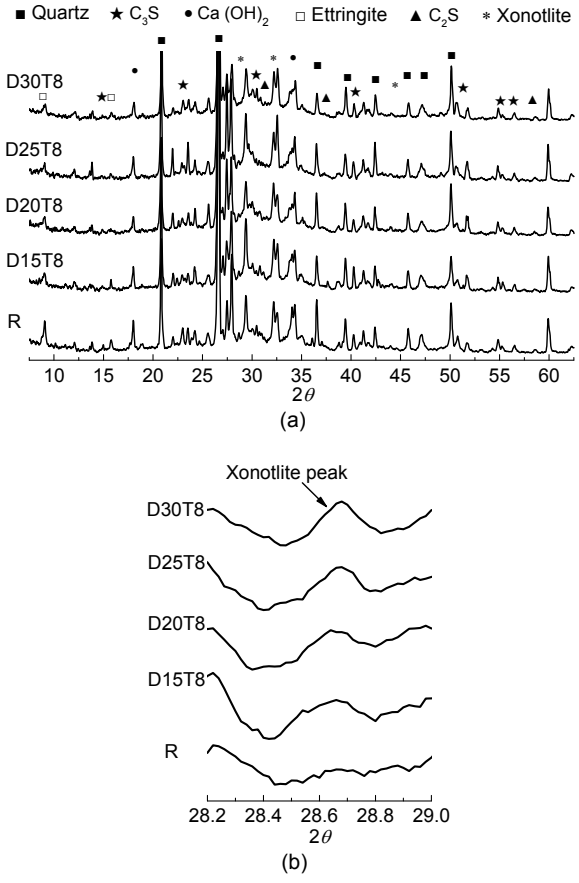

Fig. 6 XRD patterns of RPC samples (a) and Xonotlite peak (b) at day 7

In the process of high-temperature curing, the water content of the phases decreased with an increase in temperature and the C–S–H crystallized to tobermorite (Cheyrezy et al., 1995; Glasser and Hong, 2003). Then, the formation of xonotlite and gyrolite from tobermorite was visible at 200 °C (Luke, 2004), as shown in Eq. (2):

$$8\,\text{Tobermorite} \rightarrow 4\,\text{Xonotlite} + \text{Gyrolite} + 18\,H_2O. \quad (2)$$

Xonotlite was found to be one of the major crystalline hydrates in RPC at high temperature. However, Fig. 6b shows that no xonotlite peaks were observed in the control sample. After high-temperature treatment, xonotlite could be formed, and the peaks characteristic of xonotlite increased slightly. These experiment results also agree with previous research.

4 Discussion

Owing to its superior performance, RPC has a wide range of applications in civil engineering. Improving the manufacturing speed and lowering the costs of RPC are conducive to its application in practical engineering. The results of previous studies and the present research are compared in Table 6. Hot water, steam or autoclave curing generally has beneficial effects on the mechanical properties of RPC. The minimum condition for ensuring the specified early age strength derived in previous studies is a curing period of 24–48 h with a temperature of 60–100 °C under moist conditions (Teichmann and Schmidt, 2004). When the curing temperature is around 200 °C, the 7-d compressive strength of RPC exceeds 160 MPa after 2 d conservation (Prem et al., 2015).

Although the hot water, steam, and autoclave curing regimes improve the early age strength of RPC observably, these methods still take a long curing time. According to this study, the specified 7-d compressive strength of RPC can be obtained in only 8 h by using a dry-heat curing regime, which takes only one-sixth of the traditional high-temperature curing time. Therefore, the production efficiency of precast RPC components can be greatly improved by this curing method, and it may also help reduce energy consumption.

It is believed that higher curing temperatures cause a faster development of shrinkage and increase the cracking risk but, in fact, none of the specimens cured at a high temperature cracked during the test period. In general, concrete shrinkage is closely related to the shrinkage of the cement-paste phase. Some researchers have reported that the shrinkage of cement paste can be reduced substantially with a high curing temperature, and the strain measured after rewetting indicated that the reduction was primarily associated with the recoverable and irrecoverable components of shrinkage (Parrott, 1977; Juenger and Jennings, 2002; Thomas and Jennings, 2010). The RPC matrix was mainly composed of hardened cementitious materials, quartz sand, and steel fiber. The aggregate and steel fiber deformed slightly when the RH of the environment changed, whereas the hardened cementitious materials were easy to deform. On the other hand, RPC has a dense microstructure and low-porosity, which impedes the migration of moisture. Tennis and Jennings (2000) and Juenger and Jennings (2002) proposed that two types of C–S–H exist in hydrated products, i.e. high density (HD) C–S–H and low density (LD) C–S–H, and the ratio of LD C–S–H to HD C–S–H has a strong impact on the drying shrinkage. Compression stress is exerted on the pore walls when the water evaporates from the capillary pores, which causes the solid material to contract. The quartz sand, HD C–S–H, and unhydrated cement cannot deform during this contraction. Instead, capillary pores and LD C–S–H allow the restraining phases to come closer together during the drying period. It should be noted that the effect of high-temperature curing on the formation of hydration products is also crucial. Heat treatment favored the formation of denser hydration phases and increased the proportion of HD C–S–H in solid hydrates, thereby leading to a reduction of the overall gel porosity (Vandamme et al., 2010).

Fig. 7 shows a schematic diagram of the RPC matrix drying shrinkage with high-temperature curing. Compared with the control group, the hydration products achieve a higher density and stiffness with high-temperature treatment, thereby reducing the drying shrinkage of RPC. This explains why the

Table 6 Comparison of the results with previous studies

W/C ratio/ mineral admixture (cement ratio)	Specimen (mm)	Fiber volume ratio (%)	Curing temperature (°C)	Curing time	Moisture condition	Compressive strength (MPa)	Reference
0.2/Silica fume (20%)	Cylinder (Φ100×200)	1.5%–2%	60	2 d	Steam	180 (at day 7)	Park et al., 2015
0.27/Silica fume (30%)	Not specified	0%	65	1 d	Water	200 (at 5 d)	Schachinger et al., 2008
Not specified	Not specified	Not specified	70	2 d	Water	180 (at day 7)	Ishii et al., 2008
0.22/Silica fume (25%)	Cubic (100×100×100)	2%	90	2 d	Moist	202 (at day 28)	Cwirzen et al., 2008
0.22/Silica fume (25%)	Not specified	2.5%	90	2 d	Water	213 (at day 28)	Teichmann and Schmidt, 2004
0.22/Silica fume (25%)	Cubic (70×70×70)	2%	200	2 d	Moist	160 (at day 7)	Prem et al., 2015
0.40/Silica fume (42%)	Cubic (40×40×40)	0%	240	2 d	Dry	85 (at day 7)	Helmi et al., 2016
0.22/Silica fume (20%)	Cubic (70×70×70)	2%	200	4 h	Dry	160 (at day 7)	This study
0.22/Silica fume (20%)	Cubic (70×70×70)	2%	250	8 h	Dry	171 (at day 7)	This study

ultimate shrinkage of high-temperature cured RPC at 50% RH was lower than that of the control group. The drying shrinkage is associated with the reversible and irreversible components of the cement hydrate. Upon rewetting, the volume of the capillary pores was mostly recovered, whereas the volume of the LD phase is partly recovered (Juenger and Jennings, 2002). It can also be seen from Fig. 4 and Table 5 that the ultimate shrinkage of high-temperature cured RPCs at 90% RH is lower than that at 50% RH. However, the curing temperature used in this study was much higher than that of a traditional curing regime, and thus further work on the shrinkage properties of RPC cured at elevated temperatures is needed.

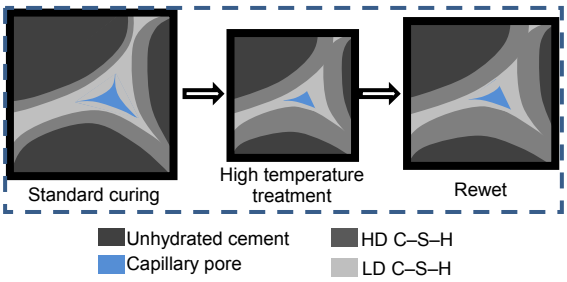

Fig. 7 Schematic diagram of RPC shrinkage with different curing regimes

5 Conclusions

1. In this study, a dry heating curing regime for improving mechanical properties of RPC was investigated, and a curing temperature of 200–250 °C and a curing time of 8 h were found to be the appropriate conditions for this regime. Compared with the traditional curing method, the strength development of RPC at early age was significantly accelerated, and the 7-d compressive and flexural strengths of RPC could exceed 170 MPa and 35 MPa, respectively.

2. A remarkable increase in early age drying shrinkage of RPC was observed as a result of dry-heat treatment. However, the ultimate drying shrinkage of specimens was effectively reduced under low RH conditions. Compared with the control group, the ultimate shrinkage of heat-treated RPC was decreased by more than 40%.

3. SEM and XRD results showed that high-temperature curing improves the microscopic pore structure of RPC, thereby making the interfacial transition zone denser; in addition, xonotlite and

tobermorite were found in the crystalline hydrates at high temperatures.

References

ACI (American Concrete Institute), 1997. Prediction of Creep, Shrinkage, and Temperature Effects in Concrete Structures, ACI 209R. ACI, USA.

ASTM (American Society for Testing Materials International), 2006. Standard Test Method for Flexural Toughness and First-crack Strength of Fiber-reinforced Concrete (Using Beam with Third-point Loading), ASTM C1018. ASTM, West Conshohocken, USA.

Aydın S, Yazıcı H, Baradan B, 2008. High temperature resistance of normal strength and autoclaved high strength mortars incorporated polypropylene and steel fibers. *Construction and Building Materials*, 22(4):504-512. https://doi.org/10.1016/j.conbuildmat.2006.11.003

Beglarigale A, Yalçınkaya Ç, Yiğiter H, et al., 2016. Flexural performance of SIFCON composites subjected to high temperature. *Construction and Building Materials*, 104: 99-108. https://doi.org/10.1016/j.conbuildmat.2015.12.034

Chen TF, Gao XJ, Ren M, 2018. Effects of autoclave curing and fly ash on mechanical properties of ultra-high performance concrete. *Construction and Building Materials*, 158:864-872. https://doi.org/10.1016/j.conbuildmat.2017.10.074

Cheyrezy M, Maret V, Frouin L, 1995. Microstructural analysis of RPC (reactive powder concrete). *Cement and Concrete Research*, 25(7):1491-1500. https://doi.org/10.1016/0008-8846(95)00143-Z

Cwirzen A, Penttala V, Vornanen C, 2008. Reactive powder based concretes: mechanical properties, durability and hybrid use with OPC. *Cement and Concrete Research*, 38(10):1217-1226. https://doi.org/10.1016/j.cemconres.2008.03.013

Felicetti R, Gambarova PG, Sora MPN, et al., 2000. Mechanical behaviour of HPC and UHPC in direct tension at high temperature and after cooling. Fifth RILEM Symposium on Fibre-Reinforced Concrete BEFIB, p.749-758.

Garas VY, Kahn LF, Kurtis KE, 2009. Short-term tensile creep and shrinkage of ultra-high performance concrete. *Cement and Concrete Composites*, 31(3):147-152. https://doi.org/10.1016/j.cemconcomp.2009.01.002

Glasser FP, Hong SY, 2003. Thermal treatment of C–S–H gel at 1 bar H_2O pressure up to 200 °C. *Cement and Concrete Research*, 33(2):271-279. https://doi.org/10.1016/S0008-8846(02)00959-6

Habel K, Charron JP, Denarié E, et al., 2006. Autogenous deformations and viscoelasticity of UHPFRC in structures. Part I: experimental results. *Magazine of Concrete Research*, 58(3):135-145. https://doi.org/10.1680/macr.2006.58.3.135

Helmi M, Hall MR, Stevens LA, et al., 2016. Effects of high-pressure/temperature curing on reactive powder concrete microstructure formation. *Construction and Building Materials*, 105:554-562. https://doi.org/10.1016/j.conbuildmat.2015.12.147

Hwang C, Young JF, 1984. Drying shrinkage of Portland cement pastes I. Microcracking during drying. *Cement and Concrete Research*, 14(4):585-594. https://doi.org/10.1016/0008-8846(84)90136-4

Ishii T, Nishio H, Matsuyama T, et al., 2008. Manufacture and construction of a PC through girder type pedestrian bridge using ultra high strength fiber reinforced concrete. Proceedings of the 8th International Symposium on Utilization of High-strength and High-performance Concrete, p.27-29.

ISO (International Organization for Standardization), 1989. Methods of Testing Cements–Determination of Strength, ISO 679:1989. ISO, Geneva, Switzerland.

Juenger MCG, Jennings HM, 2002. Examining the relationship between the microstructure of calcium silicate hydrate and drying shrinkage of cement pastes. *Cement and Concrete Research*, 32(2):289-296. https://doi.org/10.1016/S0008-8846(01)00673-1

Lehmann C, Fontana P, Müller U, 2009. Evolution of phases and micro structure in hydrothermally cured ultra-high performance concrete (UHPC). *In*: Bittnar Z, Bartos PJM, Němeček J, et al. (Eds.), Nanotechnology in Construction 3. Springer, Berlin, Germany, p.287-293. https://doi.org/10.1007/978-3-642-00980-8_38

Li HD, Xu SL, 2016. Rate dependence of ultra high toughness cementitious composite under direct tension. *Journal of Zhejiang University-SCIENCE A (Applied Physics & Engineering)*, 17(1):417-426. https://doi.org/10.1631/jzus.A1600031

Li WG, Huang ZY, Hu GQ, et al., 2017. Early-age shrinkage development of ultra-high-performance concrete under heat curing treatment. *Construction and Building Materials*, 131:767-774. https://doi.org/10.1016/j.conbuildmat.2016.11.024

Luke K, 2004. Phase studies of pozzolanic stabilized calcium silicate hydrates at 180 °C. *Cement and Concrete Research*, 34(9):1725-1732. https://doi.org/10.1016/j.cemconres.2004.05.021

Massidda L, Sanna U, Cocco E, et al., 2001. High pressure steam curing of reactive-powder mortars. *Special Publication*, 200:447-464.

Mostofinejad D, Nikoo MR, Hosseini SA, 2016. Determination of optimized mix design and curing conditions of reactive powder concrete (RPC). *Construction and Building Materials*, 123:754-767. https://doi.org/10.1016/j.conbuildmat.2016.07.082

Park JS, Kim YJ, Cho JR, et al., 2015. Early-age strength of ultra-high performance concrete in various curing conditions. *Materials*, 8(8):5537-5553. https://doi.org/10.3390/ma8085261

Parrott LJ, 1977. Recoverable and irrecoverable deformation

of heat-cured cement paste. *Magazine of Concrete Research*, 29(98):26-30. https://doi.org/10.1680/macr.1977.29.98.26

Peng GF, Kang YR, Huang YZ, et al., 2012. Experimental research on fire resistance of reactive powder concrete. *Advances in Materials Science and Engineering*, 2012: 860303. https://dx.doi.org/10.1155/2012/860303

Prem PR, Ramachandra MA, Bharatkumar BH, 2015. Influence of curing regime and steel fibres on the mechanical properties of UHPC. *Magazine of Concrete Research*, 67(18):988-1002. https://doi.org/10.1680/macr.14.00333

Reda MM, Shrive NG, Gillott JE, 1999. Microstructural investigation of innovative UHPC. *Cement and Concrete Research*, 29(3):323-329. https://doi.org/10.1016/S0008-8846(98)00225-7

Richard P, 1994. Reactive powder concretes with high ductility and 200-800 MPa compressive strength. *ACI Spring Conversion*, 114:507-517.

Schachinger I, Hilbig H, Stengel T, 2008. Effect of curing temperature at an early age on the long-term strength development of UHPC. 2nd International Symposium on Ultra High Performance Concrete, p.205-213.

Shaheen E, Shrive N, 2006. Optimization of mechanical properties and durability of reactive powder concrete. *Materials Journal*, 103(6):444-451. https://doi.org/10.14359/18222

Shen PL, Lu LN, He YJ, et al., 2018. Experimental investigation on the autogenous shrinkage of steam cured ultra-high performance concrete. *Construction and Building Materials*, 162:512-522. https://doi.org/10.1016/j.conbuildmat.2017.11.172

Shi C, Wu ZM, Xiao JF, et al., 2015. A review on ultra high performance concrete: Part I. Raw materials and mixture design. *Construction and Building Materials*, 101:741-751. https://doi.org/10.1016/j.conbuildmat.2015.10.088

Soliman AM, Nehdi ML, 2011. Effect of drying conditions on autogenous shrinkage in ultra-high performance concrete at early-age. *Materials and Structures*, 44(5):879-899. https://doi.org/10.1617/s11527-010-9670-0

Tai YS, Pan HH, Kung YN, 2011. Mechanical properties of steel fiber reinforced reactive powder concrete following exposure to high temperature reaching 800 °C. *Nuclear Engineering and Design*, 241(7):2416-2424. https://doi.org/10.1016/j.nucengdes.2011.04.008

Tam CM, Tam VWY, 2013. Microstructural behaviour of reactive powder concrete under different heating regimes. *Magazine of Concrete Research*, 64(3):259-267. https://doi.org/10.1680/macr.2012.64.3.259

Tam CM, Tam VWY, Ng KM, 2010. Optimal conditions for producing reactive powder concrete. *Magazine of Concrete Research*, 62(10):701-716. https://doi.org/10.1680/macr.2010.62.10.701

Tam CM, Tam VWY, Ng KM, 2012. Assessing drying shrinkage and water permeability of reactive powder concrete produced in Hong Kong. *Construction and Building Materials*, 26(1):79-89. https://doi.org/10.1016/j.conbuildmat.2011.05.006

Teichmann T, Schmidt M, 2004. Influence of the packing density of fine particles on structure, strength and durability of UHPC. First International Symposium on Ultra High Performance Concrete, p.313-323.

Tennis PD, Jennings HM, 2000. A model for two types of calcium silicate hydrate in the microstructure of Portland cement pastes. *Cement and Concrete Research*, 30(6): 855-863. https://doi.org/10.1016/S0008-8846(00)00257-X

Thomas JJ, Jennings HM, 2010. Effect of heat treatment on the pore structure and drying shrinkage behavior of hydrated cement paste. *Journal of the American Ceramic Society*, 85(9):2293-2298. https://doi.org/10.1111/j.1151-2916.2002.tb00450.x

Vandamme M, Ulm FJ, Fonollosa P, 2010. Nanogranular packing of C–S–H at substochiometric conditions. *Cement and Concrete Research*, 40(1):14-26. https://doi.org/10.1016/j.cemconres.2009.09.017

Wang DH, Shi CJ, Wu ZM, et al., 2015. A review on ultra high performance concrete: Part II. Hydration, microstructure and properties. *Construction and Building Materials*, 96: 368-377. https://doi.org/10.1016/j.conbuildmat.2015.08.095

Yalçınkaya Ç, Yazıcı H, 2017. Effects of ambient temperature and relative humidity on early-age shrinkage of UHPC with high-volume mineral admixtures. *Construction and Building Materials*, 144:252-259. https://doi.org/10.1016/j.conbuildmat.2017.03.198

Yanni G, Youssef V, 2009. Multi-scale Investigation of Tensile Creep of Ultra-high Performance Concrete for Bridge Applications. PhD Thesis, Georgia Institute of Technology, Georgia, USA.

Yazıcı H, Yardımcı MY, Yiğiter H, et al., 2010. Mechanical properties of reactive powder concrete containing high volumes of ground granulated blast furnace slag. *Cement and Concrete Composites*, 32(8):639-648. https://doi.org/10.1016/j.cemconcomp.2010.07.005

Yoo DY, Park JJ, Kim SW, et al., 2013. Early age setting, shrinkage and tensile characteristics of ultra high performance fiber reinforced concrete. *Construction and Building Materials*, 41:427-438. https://doi.org/10.1016/j.conbuildmat.2012.12.015

Zdeb T, 2017. An analysis of the steam curing and autoclaving process parameters for reactive powder concretes. *Construction and Building Materials*, 131:758-766. https://doi.org/10.1016/j.conbuildmat.2016.11.026

Zheng WZ, Li HY, Wang Y, 2012. Compressive behaviour of hybrid fiber-reinforced reactive powder concrete after high temperature. *Materials & Design*, 41:403-409. https://doi.org/10.1016/j.matdes.2012.05.026

中文概要

题　目： 干热养护对活性粉末混凝土力学及收缩影响研究

目　的： 高温干热养护工艺对活性粉末混凝土的力学强度及收缩性能有重要影响。本文针对不同的高温养护温度和时间分析活性粉末混凝土材料的抗压强度、抗折强度、收缩和微观结构，探索高温干热养护环境提升活性粉末混凝土材料力学性能的机理，并讨论外部环境湿度对材料收缩变形的影响。

创新点： 1. 通过调整不同养护工艺参数，大幅度提升活性粉末混凝土的早期强度；2. 建立试验模型，成功模拟适应性冲压工艺过程。

方　法： 1. 通过实验分析，研究不同养护温度和养护时间对活性粉末混凝土力学强度的影响（表 4）；2. 通过设计不同的养护湿度（50%和 90%），构建后期养护环境与材料干燥收缩之间的关系，得到适应性的后期养护参数（表 5）；3. 通过与已有研究的分析对比，提出适用于工程实际的高温干热养护工艺参数，并得出后期高湿度养护降低活性粉末混凝土收缩的微观机理（图 7）。

结　论： 1. 通过调整高温养护的温度和养护时间可以对活性粉末混凝土的强度产生影响。2. 试件在经历高温养护后再进行高湿度养护可以有效降低材料的后期干燥收缩。3. 材料界面过渡区在高温养护条件下变得更加密实；在高温环境下生成托勃莫来石或硬硅钙石是材料获得较高强度的主要原因。

关键词： 活性粉末混凝土；高温养护；力学性能；收缩